Oliver Reutter

Elena Smirnova

Jörg Sauerhering

Institute of Technical Thermodynamics,
DLR,
Köln, Germany

Stefanie Angel
Department of Ferrous Metallurgy,
Aachen University,
52060 Aachen, Germany

Thomas Fend

Robert Pitz-Paal

Institute of Technical Thermodynamics,
DLR, Köln,
Germany

Characterization of Air Flow Through Sintered Metal Foams

This study investigates air flow in metallic foams, which are produced by the slip reaction foam sintering (SRFS) process. It was conducted as part of the collaborative research center (SFB) 561 "Thermally Highly Loaded, Porous and Cooled Multi-Layer Systems for Combined Cycle Power Plants." The flow through a porous medium is analyzed by Darcy's equation with the Dupuit/Forchheimer extension. All measurements can be described very well by this equation and permeability and inertial coefficients are obtained for a large quantity of samples with different base materials and different porosities. A threshold porosity of 70% is observed, above which the pressure loss significantly starts sinking with porosity. Additionally, it was found that the permeability was anisotropic. Permeability is lower in the direction of gravity during foaming. Scattering in the data of the permeability and inertial coefficients versus the porosity is observed and discussed.
[DOI: 10.1115/1.2907419]

1 Introduction

The foams investigated in the present study are produced by the slip reaction foam sintering (SRFS) process. This is a promising method to produce open porous metallic foams. This process produces the porous cell structure by a chemical reaction process. In comparison to other production routes for metallic foams, the SRFS method provides several advantages as it allows working at room temperature and results in foams with a great variety of density pore size and pore shape. A wide range of base materials, such as iron, iron base, and nickel base alloys, can be supplied. As this foaming is a rather new method, there is not yet ready available data concerning the pore structure or the behavior to fluid flow. The foam structure is not similar to the foams made by casting using a polymer precursor as template or by metal deposition on cellular performs, such as polyurethane foams [1]. Therefore, it was necessary to conduct a series of extensive experiments in order to characterize the SRFS foams. A first introduction and first results have been published at the fourth International Conference on Nanochannels, Microchannels and Minichannels [2].

These foams promise a wide range of applications because there is a big choice of base materials and porosity. One promising application is the use of foam as an open wall element of combustion chambers. This topic is investigated within the collaborative research center (SFB) 561 "Thermally Highly Loaded, Porous and Cooled Multi-Layer Systems for Combined Cycle Power Plants." It aims at increasing the efficiency of the gas turbine by raising the gas temperature.

Within this research center, the present study was carried out. Increasing the temperature leads to the necessity of actively cooling the combustion chamber walls by effusion cooling, which means that cooling air is pressed through little holes into the chamber. The metallic foam is intended to be coated with a thermal barrier layer with laser drilled bore holes and used as a combustion chamber wall element [3,4]. The knowledge of the temperature distribution inside the wall element (foam+coating) is important to predict the lifetime of the materials employed. To predict the temperature, flow through the wall element has to be characterized. For this, experimental data on the heat transfer characteristics, the thermal conductivity, and the pressure drop characteristics are needed. The last property is subject of the present study.

2 Investigated Materials

The base of the technique is a metal suspension [5,6]. Fine metallic powders are mixed with a dispersant, solvent, and concentrated phosphoric acid as binder. The phosphoric acid forms a metal phosphate together with the metallic particles and hydrogen is set free by the reaction between the metallic particles and the acid. The metal phosphate freezes the hydrogen bubbles in the slip. After drying, the samples are sintered under defined, reducing conditions and as the solvent evaporates, an open porous structure with the porosity in the range of 62–87% is received. The process provides a wide range of process parameters, which allow adjusting the foam structure concerning density, pore size, and pore shape distribution to influence the mechanical and flow properties. Graded structures can be supplied. The scheme for obtaining such foams can be seen in Fig. 1.

The investigated samples for this study are made of Hastelloy B, Inconel 625, and NC-powder. The grain sizes range between 50 μm and 150 μm. The densities of the bulk material, the metal powder particles, and the apparent density are compiled in Table 1. The iron based samples (NC) were sintered at 1170°C for 60 min with a heating rate of 8 K/min, and the nickel based samples (Inconel 625 and Hastelloy B) at 1200°C for 60 min. Two intermediate temperature levels were set in the case of the nickel based samples during heating up, one at 150°C and the second at 350°C, to guarantee that the escaping water vapor will be moved out of the furnace. The heating rate was 3 K/min until 350°C and then 8 K/min. After evacuating the furnace one time before starting the sintering process, the samples were sintered under a reducing atmosphere of 100% H_2.

Contributed by the Fluids Engineering Division of ASME for publication in the JOURNAL OF FLUIDS ENGINEERING. Manuscript received December 18, 2006; final manuscript received March 6, 2008; published online April 25, 2008. Assoc. Editor: Timothy J. O'Hern.

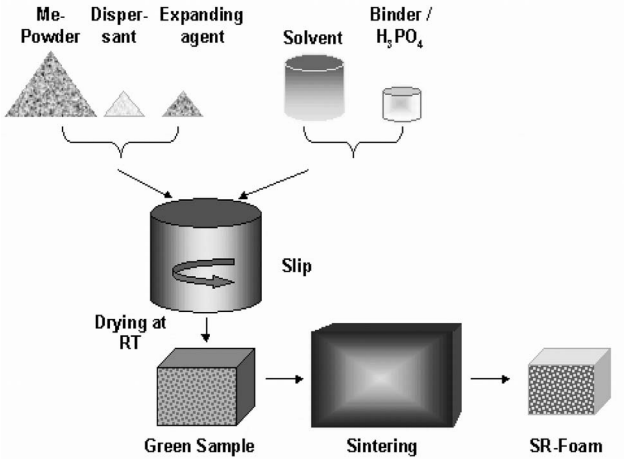

Fig. 1 Scheme of the SRFS process

Samples made only of the sintered slip without foaming show a porosity of about 50% (densities of 3.8–4.2 g/cm^3) and are called *sintered powder samples*. These samples are taken as representing the material of the pore walls in the foams. The foams have a total porosity between 62% and 87% (densities of 1.2–3.7 g/cm^3). The pores can be characterized as those that arise from the hydrogen foaming, called the primary pores, and those that are the spaces between adjacent grains of the sintered powder, called the secondary pores [7]. The secondary pores reach up to 0.3 mm diameter and the primary pores reach up to 3.5 mm.

All densities were determined as gravimetrical densities by weighing the foam samples, and dividing this weight by the total volume of the foam sample, which was calculated from measurements with a sliding caliper. The total porosity was determined by using the density of the bulk material as the reference.

The samples were produced at the Department of Ferrous Metallurgy at Aachen University. The samples are cylinders with diameters between 64 mm and 81 mm and the length was between 9 mm and 30 mm. The picture of a typical sample can be seen in Fig. 2 (left) together with an optical micrograph of the sample (right). For measurements of anisotropy effects, cubical samples were used with 45 mm side length.

Table 1 Overview of the densities of the powder material

	Density of the bulk material (g/m^3)	Density of the powder particles	Apparent density of the powder
NC	7.87	7.76	2.45
Hastelloy B	9.24	Not determined	Not determined
Inconel 625	8.44	8.10	2.84

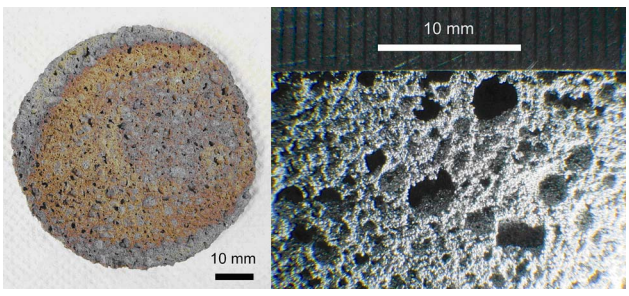

Fig. 2 Picture of a sample of a Hastelloy B foam and a detailed view of the pore structure

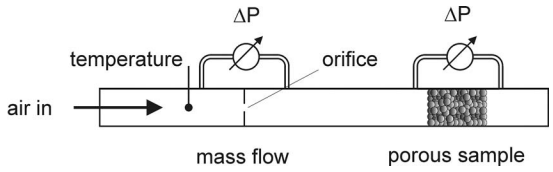

Fig. 3 Experimental setup for measuring the pressure drop of the samples (schematic)

3 Permeability and Experimental Setup

Referring to publications by Innocentini et al. [8], Boomsma et al. [9], Boomsma and Poulikakos [10], and Lage et al. [11,12], it is useful to describe the flow through a porous medium in terms of Darcy's equation with the Dupuit/Forchheimer extension (Eq. (1)) and not only by Darcy's equation. It is applicable, if the flow through a porous medium is not very low. As it fits the experimental data very well, only the extended equation was used in this study:

$$\frac{dP}{dx} = \frac{\eta_{\text{dyn}}}{K_1} v + \frac{\rho}{K_2} v^2 \tag{1}$$

Since the air flow velocity v and the differential pressure loss dP/dx are not constant along the path of the (compressible) fluid through the porous sample, an expression for dP/dx at the outlet of the flow from the sample is needed, because at this location the air flow velocity $v=v_o$ is determined. For the determination of v, the mass flow $\dot{M}$ is needed, which is constant throughout the tubing and which is measured. Furthermore, the air density ρ_o is needed, so the velocity may be calculated with the cross-sectional area A according to

$$v_o = \frac{\dot{M}}{\rho_o A}$$

Air density data are taken from the tables using the temperature (T_o) and pressure data (P_o) at the outlet of the flow through the sample [13]. v_o is understood as the velocity, which one would have in a 100% porous sample (superficial velocity).

The needed expression for the differential pressure loss dP/dx is $P_i^2 - P_o^2/2P_oL$, so Eq. (1) may be rewritten for the case at the outlet location as

$$\frac{dP_o}{dx} = \frac{P_i^2 - P_o^2}{2P_oL} = \frac{\eta_{\text{dyn}}}{K_1} v_o + \frac{\rho_o}{K_2} v_o^2 \tag{2}$$

After plotting the data with different flow velocities and performing a second order polynomial fit, once more air density data are needed to extract K_2 from the coefficients of the fit. In this case, also ρ_o is taken, which remains nearly constant for various v_o throughout the duration of the test series, which usually takes an hour or shorter. Accordingly, K_1 is calculated with temperature dependent air viscosity data from Ref. [14]. In this way, K_1 and K_2 are acquired as material constants independent of the fluid, pressure, and temperature environment.

The experimental setup is shown in Fig. 3. A fan drives an air flow through a metal tube array. The mass flow rate was calculated from the pressure difference between two sensors before and behind a defined orifice, the absolute pressure, and the air temperature assuming a relative humidity of 50% at room temperature for the air density. The pressure drop across the sample was measured together with the air temperature close to the sample position. The orifice plate has been manufactured by Mangels (Wilhelmshafen, Germany) and the difference pressure sensors used were a DPI 260 by Druck (Germany) and a MaPress by Madur (Austria). The absolute pressure of the air in the laboratory was measured for each experiment and varied between 985 mbars and 1032 mbars depending on the weather. The experiment takes

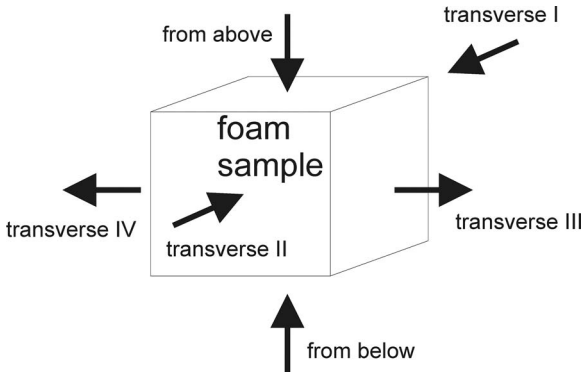

Fig. 4 Sketch of the possible air flow directions in a cubic sample. Above and below can be distinguished in the sample, because of the direction of the gravity during the foaming and drying process.

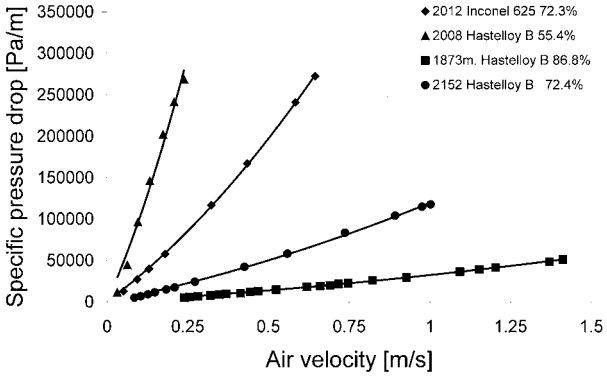

Fig. 5 Pressure drop measurements of samples with different densities

place at air temperatures slightly above room temperature caused by heat losses of the blower. Typical values for viscosity and air density are $1.82\ 10^{-5}$ Pa s and $1.21\ \mathrm{kg/m^3}$, respectively. The round sample was tightly inserted in a metal pipe with some layers of flexible foamed rubber around it. The air tightness of this sample holding was tested by inserting an impermeable block of steel with similar dimensions, as the samples in the sample holder and at maximum fan power only detecting a negligible mass flow. The area exposed to the flow varied between 32 $\mathrm{cm^2}$ and 52 $\mathrm{cm^2}$ for the cylindrical samples and 20 $\mathrm{cm^2}$ for the cubic samples.

The accuracy of the specific pressure drop measurements is dominated by the accuracy of the difference pressure measurements for low values of the specific pressure drop and by the accuracy of the measurement of the sample thickness for high values. So for measurements above 25,000 Pa/m, an error of about $\pm 5\%$ can be assumed, which rises for lower values and can reach values above 10%. For the velocity measurements, the error at low velocities is dominated by the accuracy of the difference pressure drop measurement over the orifice, while at high velocities, the geometric error of the superficial area dominates. The influence of the accuracy of the absolute pressure and temperature measurements is not very high. So above a velocity of 0.2 m/s, an uncertainty of approximately $\pm 5\%$ is realized, which significantly rises for lower velocities and can reach values above 40% for 0.05 m/s. As discussed by Innocentini et al. [15], the validity of the permeability coefficients is strictly restricted to the flow velocity regime occurring during measurement. Additionally, though the overall accuracy of pressure drop is comparably high for most samples (approximately $\pm 5\%$ along with $\pm 5\%$ uncertainty of the velocity) and the measurements can be very well fitted by a second order polynomial function, the uncertainty of the single coefficients K_1 and K_2 is higher, also because they are not independent of each other during fitting.

In order to investigate anisotropy effects, cubic samples have been manufactured. They are subjected to air flow in six different directions. During the process of foaming and drying, there is only one distinct direction, that of gravity. The samples were carefully prepared, so the direction during measurements was defined. For a sketch of the possible air flow directions, see Fig. 4.

4 Results

As examples, two plots of the pressure difference as a function of air velocity are presented in the Figs. 5 and 6. Figure 5 contains curves of foams with various densities. Figure 6 shows the results of the anisotropy investigations. The quadratic dependency of the pressure drop on flow velocity can be clearly seen. The second order polynomial function fits match the measured data very well, so the applicability of Eq. (1), from which the permeability coefficient K_1 and the inertial coefficient K_2 may be derived, is obvious. As the absolute pressure on the entrance of the tube array is limited by the experimental equipment, the velocity range of the measurements is limited, too. Consequently, the denser the sample, the smaller the velocity range of the measurement. The sintered powder samples, which have no primary porosity, were investigated at velocities of up to 0.2 m/s (left curve in Fig. 5).

In Fig. 5, we also see the dependency of the pressure drop on the velocity for the samples with different densities. As expected, the denser samples show higher pressure drops. The samples' density range varies from porous material, which was made out of only sintered powder metal (porosity $\varepsilon \approx 50\%$, density $\rho \approx 4\ \mathrm{g/cm^3}$) and foams, which were foamed ($\varepsilon \approx 87\%$, $\rho \approx 1.2\ \mathrm{g/cm^3}$). As base material, samples with Inconel 625, Hastelloy B and NC powder were used.

In Fig. 6, we see an example of an anisotropy measurement for an Inconel 625 sample. For this measurement, a cubic sample was used. Of the six possible directions of air flow in a cube, the result shows us groups of two different pressure drops. For the foaming direction, a higher pressure drop is observed compared to the transverse directions. A possible explanation of this is that there are more connections between the pores transverse to the foaming direction, and another one that the pores might be elongated transverse to the foaming direction. Most probably, it is a combination of both. At the moment, there are not yet enough optical investigations of the pore structure to decide this.

All investigated cubic samples showed the same behavior. For the further study of the pressure drop characteristics, round samples were used. All of these were subjected to an air flow in the foaming direction.

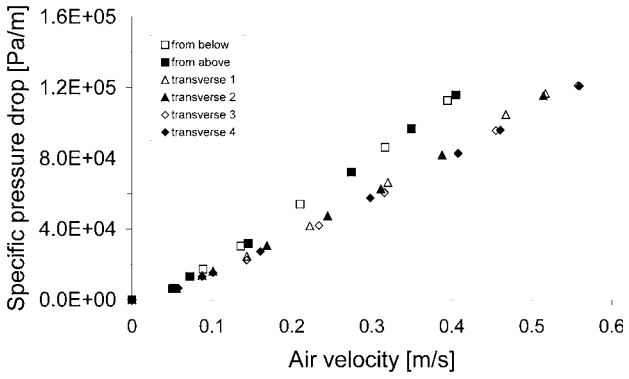

Fig. 6 Pressure drop of a cubic Inconel 625 sample in six different directions

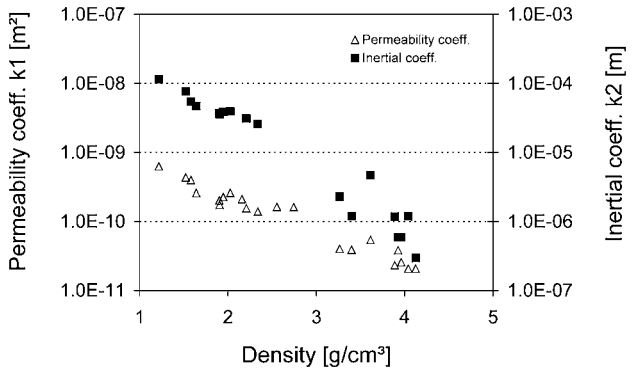

Fig. 7 Dependency of the permeability and inertial coefficients on the density of the Hastelloy B foam samples

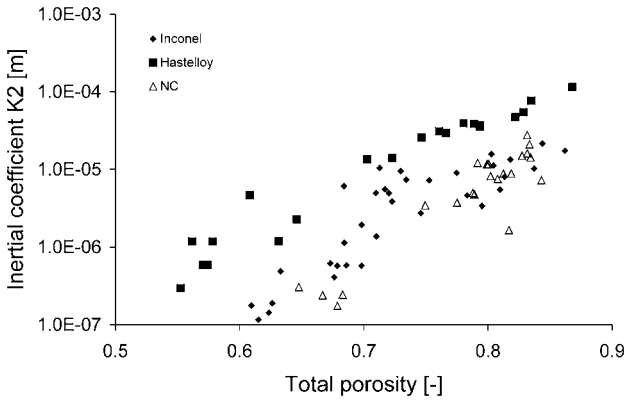

Fig. 9 Comparison of the inertial coefficients sorted by matrix material

Using the above described method for obtaining the permeability and the inertial coefficients, a large variety of samples has been measured. The results are presented for the three different material types (Inconel 625, Hastelloy B and iron (NC)).

Figure 7 shows the dependency of the permeability and inertial coefficients on the density for samples of Hastelloy B. The density of Hastelloy B as a dense material is 9.22 g/cm^3. As stated above, the densest samples were not foamed, but samples that were made by only sintering Hastelloy B powder without adding a foaming agent. A total number of five of these materials have been investigated. They have density values of approximately 4 g/cm^3. In this case, flow may be imagined as flow through a packed bed of sintered metal grains. As expected, a trend can be seen that samples with higher densities (lower porosity) show lower permeability and lower inertial coefficients. For the other materials, these dependencies are very similar; therefore we here only show the Hastelloy B results in such a diagram.

Comparisons of the obtained results for all materials are presented in the next two figures. In order to make the comparison possible, not the density (which is different for the base materials) but the total porosity is used. The data for inertial and permeability coefficients are separately presented. We see a dependency of pressure drop coefficients on total porosity in the figures. In all samples with all base materials, there is a trend to lower pressure drop at higher porosity but not a strict dependency. Samples with small difference in density can have a bigger difference in pressure drop than samples with a larger difference in density. For all materials, it is possible to find samples with about 8% difference in the total porosity and very similar permeability coefficients. It is not yet clear how to account for this effect. Possible explanations are the stochastic foaming effect, the manual laboratory scale production process, and the influence of the division of the total porosity into open, closed, and half-open porosities. The range of the iron and Inconel 625 samples pressure drop was similar. Hastelloy B sample pressure losses are smaller. This is probably an effect of the powder morphology and grain size distribution.

Furthermore, it can be seen from Fig. 8 that there is a minimum total porosity of about 70% above which permeability continuously increases. This may be explained by the primary pores forming a permeable network, whereas before primary pores are not connected by windows but only through the porous matrix walls.

Optical characterization (see Fig. 2) shows that the connections between primary pores (windows) are rather small and in the range of a few powder particle diameters, more like a small hole in a wall between pores. The walls of the primary pores are a porous sintered packed bed. This structure of the SRFS metal foam samples leads to lower permeability and inertial coefficients that one would expect from the primary pore dimensions and compared to foams on the basis of reticulated polyurethane foams with similar porosities (Fig. 9).

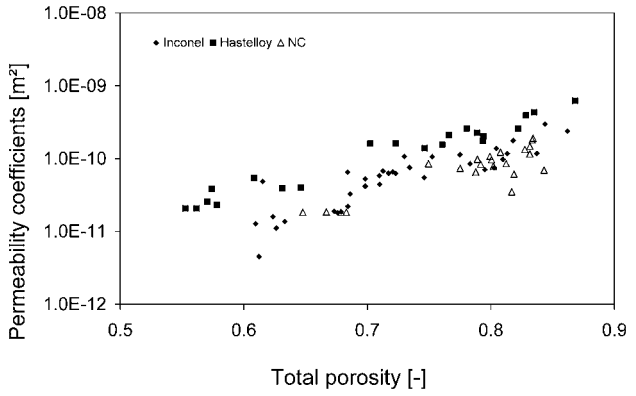

Fig. 8 Comparison of the permeability coefficients sorted by matrix material

5 Conclusions

There is a clear tendency that the higher the sample density, the lower the permeability. This corresponds to the known dependency of the permeability on porosity for other structures [3]. The results show that for the same porosity Hastelloy B samples significantly exhibit higher permeabilities than Inconel and NC samples. Anisotropy can be observed in the SRFS foams. In the direction of the foaming, the pressure drop is higher than in the transverse directions. For comparison of different densities, only data from the same flow direction were used. Above 70% total porosity, the primary pores seem to form a network. Above this porosity, there is a clear increase in permeability with increasing porosity. The data acquired on pressure drop characteristics of SRFS foams is an important tool for the manufacturer to create foams with the desired pressure drop characteristics. The design of functional elements, such as the porous combustion chamber wall of a gas turbine, may be improved.

Acknowledgment

The support of the Deutsche Forschungsgemeinschaft (DFG) for the collaborative research center "Thermally Highly Loaded, Porous and Cooled Multi-Layer Systems for Combined Cycle Power Plants" (SFB 561) is thankfully acknowledged.

Nomenclature

P = absolute fluid pressure (Pa)

ΔP = pressure difference between inlet and outlet $P_i - P_0$ (Pa)

L = length of the sample (m)
η_{dyn} = dynamic viscosity of the fluid (Pa s)
ν = superficial velocity (m/s)
ρ = density of the fluid (kg/m^3)
ε = porosity (%)
K_1 = permeability coefficient (m^2)
K_2 = inertial coefficient (m)
$\dot{M}$ = mass flow rate (kg/s)
A = cross section of the sample exposed to flow (m^2)

References

[1] Ashby, M. F., Evans., A., Fleck, N. A., Gibson, L. J., Hutchinson, J. W., and Wadley, H. N. G., 2000, *Metal Foams: A Design Guide*, Butterworth-Heinemann, Boston.

[2] Reutter, O., Sauerhering, J., Smirnova, E., Fend, Th., Angel, St., and Pitz-Paal, R., 2006, "Experimental Investigation of Heat Transfer and Pressure Drop in Porous Metal Foams," *Proceedings of ASME ICNMM2006, Fouth International Conference on Nanochannels, Microchannels and Minichannels*, Limerick, Ireland, Jun. 9–21, Paper No. ICNMM2006-96135.

[3] Bohn, D., 2002, "New Materials and Cooling Systems for High Temperature, Highly Loaded Components in Advanced Combined Cycle Power Plants," *Seventh Liege Conference on "Materials for Advanced Power Engineering*, Liege, Belgium, Sept. 30–Oct. 02.

[4] Bohn, D., and Moritz, N., 2001, "Numerical Investigation on Flow Field and Heat Transfer Phenomena in Multi-Hole Cooling Configurations," *RTO-Symposium*, Loen, May.

[5] Scholz, P.-F., 1997, Patent DE 197, 16, 514, C, 1.

[6] Angel, S., Bleck, W., and Scholz, P.-F., 2005, "Adjusting the Pore Structure of Open Porous Metallic Foams Produced by the SlipReactionFoamSintering (SRFS)—Process," *Fourth International Conference MetFoam*, Kyoto, Japan, Sept. 21–23, Japan Institute of Metals.

[7] Angel, S., Bleck, W., Scholz, P.-F., and Fend, Th., 2004, "Influence of Powder Morphology and Chemical Composition on Metallic Foams Produced by Slip-ReactionFoamSintering (SRFS)—Process," Steel Res., **75**, pp. 483–488.

[8] de Mello Innocentini, M. D., Sepulveda, P., and dos Santos Ortega, F., "Permeability," *Cellular Ceramics*, M. Scheffler and P. Colombo, eds., Wiley-VCH, Weinheim, pp. 313–341.

[9] Boomsma, K., Poulikakos, D., and Ventikos, Y., 2003, "Simulation of Flow through Open Cell Metal Foams Using an Idealized Periodic Cell Structure," Int. J. Heat Fluid Flow, **24**, pp. 825–834.

[10] Boomsma, K., and Poulikakos, D., 2002, "The Effects of Compression and Pore Size Variations on the Liquid Flow Characteristics in Metal Foams," ASME J. Fluids Eng., **124**, pp. 263–272.

[11] Lage, J. L., and Antohe, B. V., 2000, "Darcy's Experiments and the Deviation to Nonlinear Flow Regime," ASME J. Fluids Eng., **122**, pp. 619–625.

[12] Lage, J. L. et al., 2005, "Protocol for Measuring Permeability and Form Coefficient of Porous Media," Phys. Fluids, **17**, 088101.

[13] 1991, VDI-Wärmeatlas, 6. Auflage, VDI-Verlag.

[14] Bohl, W., Technische Strömungslehre, 11 durchgesehene Auflage, Vogel Buchverlag, p. 268.

[15] Innocentini, M. D. M, Salvini, V. R., Pandolfelli, V. C., and Coury, J. R., Jr., 1999, "Assessment of Forchheimer's Equation to Predict the Permeability of Ceramic Foams," J. Am. Ceram. Soc., **82**(7), pp. 1945–1948.